CCFE-PR(15)67

L. Carbajal, S. C. Chapman, R. O. Dendy, N. W. Watkins,
and J. W. S. Cook

Hybrid simulations of preferential ion heating due to intermittent magnetic fields in the solar wind

Hybrid simulations of preferential ion heating due to intermittent magnetic fields in the solar wind

L. Carbajal[1], S. C. Chapman[1, 2], R. O. Dendy[3,1], N. W. Watkins[4, 5, 6], and J. W. S. Cook[1]

[1]Centre for Fusion, Space and Astrophysics, Department of Physics, The University of Warwick, Coventry, CV4 7AL
[2]Department of Mathematics and Statistics, University of Tromsø, TromsøN-9037, Norway
[3]EURATOM/CCFE Fusion Association, Culham Science Centre, Abingdon, Oxfordshire OX14 3DB, UK
[4]Centre for the Analysis of Time Series, London School of Economics and Political Science, London WC2A 2AE, UK
[5]Max Planck Institute for the Physics of Complex Systems, Dresden D-01187, Germany
[6]Department of Engineering and Innovation, Faculty of Mathematics, Computing and Technology, The Open University, Walton Hall, Milton Keynes MK7 6AA, UK

Hybrid Simulations of Preferential Ion Heating Due to Intermittent Magnetic Fields in the Solar Wind

L. Carbajal

Centre for Fusion, Space and Astrophysics, Department of Physics, The University of Warwick, Coventry CV4 7AL, UK

L.Carbajal-Gomez@warwick.ac.uk

S. C. Chapman

Centre for Fusion, Space and Astrophysics, Department of Physics, The University of Warwick, Coventry CV4 7AL, UK

Department of Mathematics and Statistics, University of Tromsø, TromsøN-9037, Norway

R. O. Dendy

EURATOM/CCFE Fusion Association, Culham Science Centre, Abingdon, Oxfordshire OX14 3DB, UK

Centre for Fusion, Space and Astrophysics, Department of Physics, The University of Warwick, Coventry CV4 7AL, UK

N. W. Watkins

Centre for the Analysis of Time Series, London School of Economics and Political Science, London WC2A 2AE, UK

Max Planck Institute for the Physics of Complex Systems, Dresden D-01187, Germany

Centre for Fusion, Space and Astrophysics, Department of Physics, The University of Warwick, Coventry CV4 7AL, UK

Department of Engineering and Innovation, Faculty of Mathematics, Computing and Technology, The Open University, Walton Hall, Milton Keynes MK7 6AA, UK

and

J. W. S. Cook

Centre for Fusion, Space and Astrophysics, Department of Physics, The University of Warwick, Coventry CV4 7AL, UK

ABSTRACT

Preferential ion heating in the solar wind, observed as the occurrence of an ion beam which drifts along the background magnetic field with a velocity close to the local Alfvén speed, is still an open problem. Several mechanisms have been identified that might work together in the solar wind to drive the observed ion heating. These mechanisms result from nonlinear ion kinetic effects such as trapping by ion-acoustic waves and by parallel electric fields. Fluctuations observed in the solar wind are intermittent, which can modify the efficiency of these heating mechanisms. We

present the first study of preferential ion heating in the fast solar wind that includes intermittent electromagnetic fields in a self-consistent way. We perform fully self-consistent 1.5D hybrid simulations of an intermittent $1/f^{\gamma}$ broadband spectrum of Alfvén waves relaxing in a solar wind plasma. Our hybrid simulations treat ions as kinetic particles and electrons as a neutralizing massless fluid. We find that the temporal and spatial dynamics of the mechanisms driving preferential ion heating in our simulations, specifically, gyrobunching and ion trapping by the electric field, show strong dependence on the level of intermittency in the electromagnetic fields. We also find that the ion temperature anisotropy $T_{\perp}/T_{\parallel}$ (perpendicular temperature/parallel temperature), and the degree of correlation between velocity and magnetic field fluctuations also depend on the level of intermittency. Our results suggest that some level of intermittency must be included in self-consistent modelling of the solar wind in order to obtain values of these solar wind parameters consistent with observations.

Subject headings: Preferential ion heating, hybrid simulations, intermittent Alfvén waves, gyrobunching, particle trapping.

1. INTRODUCTION

Observations of the solar wind typically show existence of preferential heating of protons and alpha-particles along the local magnetic field. This preferential ion heating is observed in the reconstructed velocity probability distribution functions of protons and alpha-particles, which have long tails along the local magnetic field (Hundhausen et al. 1967; Gurnett et al. 1979; Marsch et al. 1982a,b; Marsch 2006). The occurrence of this anisotropic heating of ions in the fast solar wind appears to be independent of the heliocentric distance at which the solar wind velocity is measured.

Fluctuations in the fast solar wind magnetic field exhibit inverse power-law regions in the frequency domain. At higher frequencies there is an inertial range of fully developed turbulence $\sim f^{-5/3}$ (Marsch and Tu 1990; Goldstein et al. 1995; Bruno and Carbone 2013), and at low frequencies a region $\sim 1/f$ whose origin is coronal (Matthaeus and Goldstein 1986; Bruno et al. 2009; Verdini et al. 2012). The broadband spectra of coherent waves permeating the solar wind are Alfvénic in nature (Belcher and Leverett Jr. 1971; Belcher and Solodyna 1975; Bruno et al. 1985; De Pontieu et al. 2007; Bruno and Carbone 2013).

There is evidence that the inertial range fluctuations incorporate intermittent turbulence (Hnat et al. 2002; Bruno et al. 2007; Osman et al. 2011, 2012; Alexandrova et al. 2013; Wu et al. 2013; Osman et al. 2014). In addition, intermittency is also seen in fluctuations at lower frequencies in the $1/f$ range (Hnat et al. 2003; Horbury et al. 2005; Nicol et al. 2009). Here, we refer to intermittency in the most general sense as the occurrence of occasional large-amplitude fluctuations, or bursts, in the time series of the solar wind parameters. As the fast solar wind plasma propagates away from the sun, the intermittent magnetic field evolves, showing both temporal and spatial intermittency (Taylor 1938; Veltri 1999).

There has been extensive modelling and simulations of ion heating by fluctuating fields in the solar wind. Ofman (2004) studied the heating of the solar wind using a three-fluid model for the plasma. A broadband spectrum of low-frequency Alfvén waves was used to drive the heating, with initial wave-phases that depended on the latitude at which they were launched from the base of the solar corona. However, a multi-fluid model for the plasma cannot describe in detail the wave-particle interactions, nor their effects on the velocity distributions of the different ion species of the plasma. In Liewer et al. (2001); Araneda et al. (2008, 2009); Matteini et al. (2010, 2011), and more recently Maneva et al. (2013), the heating of pure proton and proton-helium plasmas due to parametric decay of a single Alfvén wave, or due to broadband spectra of Alfvén waves, was examined using hybrid simulations of the expanding solar wind plasma in one spatial dimension. In these hybrid simulations, kinetic ion dynamics is resolved in detail. Valentini et al. (2008) and Valentini and Veltri (2009), explored ion heating in solar wind plasmas driven by high-frequency Alfvén waves using hybrid Vlasov-Maxwell simulations. However, alpha-particles were not included in their simulations, which can significantly modify the plasma dynamics despite their low abundance in the solar wind plasma (Maruca et al. 2012). These studies showed the existence of mechanisms such as nonlinear ion trapping by ion-acoustic waves, resonant interaction of ions with ion cyclotron Alfvén waves, and ion trapping by parallel electric fields due to density or magnetic pressure gradients, which can drive preferential ion heating. Other studies (Nariyuki et al. 2010, 2014) have shown the occurrence of preferential ion heating driven by nonlinear Alfvén wave packets in the expanding solar wind plasma in the absence of parametric instabilities. More recently, in Perrone et al. (2013), the authors showed the occurrence of preferential ion heating of protons and alpha-particles in their simulations of two-dimensional plasma turbulence in the solar wind. Importantly, all these studies provide mechanisms and configurations of solar wind plasmas that might underlie the observed preferential ion heating in the solar wind, but intermittency is not included in their models.

We present the first study of preferential ion heating in the fast solar wind at 1 AU that explicitly includes intermittent electromagnetic fields in a self-consistent way. We investigate the effect on preferential ion heating of different levels of intermittency within $1/f^{\gamma}$ broadband spectra of Alfvén waves. We perform 1.5D hybrid simulations of the relaxation of intermittent broadband spectra of Alfvén waves in a solar wind plasma comprised

of protons and alpha-particles. We identify gyrobunching and ion trapping by the electric field as the mechanisms underlying the observed preferential ion heating, and determine the effect of intermittency on the local ion temperature and on the ion temperature anisotropy for protons and alpha-particles. We study the detailed time evolution of the fluctuations of the ion velocity and magnetic field for different scenarios with different levels of intermittency. We find that the level of intermittency of the electromagnetic fields strongly affects the temporal and spatial dynamics of the mechanisms underlying preferential ion heating, as well as temperature anisotropy of both ion species.

2. THE HYBRID SIMULATION METHOD

We employ the hybrid approximation to model the plasma in order to describe phenomena occurring on lengthscales comparable to, or greater than, the ion inertial length, and on timescales comparable to the ion gyroperiod (Winske and Omidi 1996; Clark et al. 2013). The hybrid approximation accommodates low-frequency ion kinetic waves, as well as electromagnetic modes including ion-cyclotron waves and Alfvén waves. The full three-dimensional ion dynamics are governed by the Lorentz force. The full velocity space distributions of different ion populations are evolved by following an ensemble of super-particle trajectories in phase space, and the electrons are represented as a charge-neutralizing massless fluid. The fluid electrons are modelled as an isotropic and isothermal ideal gas, $P_e = n_e T_e$, where T_e is the electron temperature. Neglecting the electron inertia term gives a relationship between the electric and magnetic fields:

$$\boldsymbol{E} = \frac{1}{\mu_0 e n_e}(\nabla \times \boldsymbol{B}) \times \boldsymbol{B} - \boldsymbol{U}_i \times \boldsymbol{B} - \frac{1}{e n_e}\nabla P_e \,. \quad (1)$$

Our 1.5D simulations evolve the full 3D vector electromagnetic fields $\boldsymbol{E}(x,t)$ and $\boldsymbol{B}(x,t)$ with variation in one spatial direction and time. We use the code described in Carbajal et al. (2014). The numerical parameters of the hybrid simulations are chosen so that they properly resolve the ion gyromotion in space and time, together with the fastest mode of the electromagnetic fields included in the hybrid approximation for the plasma (Pritchett 2000). The simulation domain consists of 4096 grid cells, which corresponds to length $L = 1024 d_p$. Where d_p is the ion inertial length. This set up offers a good trade-off between resolution and computational cost, given that $d_p \approx 3.6 r_p$ and $r_p = r_\alpha$, with r_p and r_α the proton and alpha-particle gyro-radius, respectively. For each ion species we use 400 super-particles per grid cell. In Sec. 3.1 we set up of the intermittent broadband spectra of Alfvén waves, and how the different ion species are self-consistently coupled to the waves.

3. SIMULATION SET-UP

We study the effect of different levels of intermittency and different spectral exponents γ of $1/f^\gamma$ broadband spectra of Alfvén waves on preferential ion heating in the fast solar wind. We specify both the amplitude and phase spectra of these waves as an initial condition; they are then left to freely relax in time. We test the sensitivity of simulation results to different values of the spectral exponent γ by choosing $\gamma = 0, 1,$ and $5/3$. In all the hybrid simulations presented here, we use characteristic parameters of solar wind plasmas as measured at 1 AU (Bruno and Carbone 2013). Our simulations are carried out in slab geometry, with the direction of variation parallel to the background magnetic field. The background magnetic field is $\boldsymbol{B}_0 = B_0 \hat{\boldsymbol{x}}$, with $B_0 = 6$ nT. Following Maneva et al. (2013), we consider a homogeneous plasma of thermalized majority protons and a minority population of alpha-particles with equal temperatures $T_p = T_\alpha$. The corresponding ion betas, $\beta_i = v_{th,i}^2 / V_A^2$, defined in terms of the thermal speed of each species $v_{th,i} = \sqrt{2 k_b T_i / m_i}$ and the Alfvén speed $V_A = B_0 / \sqrt{\mu_0 n m_p}$, are $\beta_\alpha \approx 0.02$ and $\beta_p \approx 0.08$, while the electron beta is $\beta_e = v_{th,e}^2 / V_A^2 \approx 0.05$. The alpha-particle concentration in all the simulations is $n_\alpha / n_e = 0.05$, which corresponds to the characteristic abundance of alpha-particles in the fast solar wind (Marsch et al. 1982a).

3.1. Set-up of the electromagnetic fields

We include intermittency in the initial $1/f^\gamma$ broadband spectrum of Alfvén waves driving the ion heating in our simulations, by initially specifying a non-random phase relationship between these waves. These waves initially satisfy the

appropriate dispersion relation of the plasma at $t\Omega_p = 0$, and together contain the same total field energy in all the simulations.

Clear evidence of broadband Alfvénic activity in the solar wind has been observed in early (Belcher and Leverett Jr. 1971; Belcher and Solodyna 1975; Bruno et al. 1985) and recent (De Pontieu et al. 2007; Bruno and Carbone 2013) studies of the solar wind, which show strong correlation between the solar wind velocity and the local magnetic field. Outward-propagating Alfvén waves dominate (Belcher and Leverett Jr. 1971). For this reason, we simplify our study of the solar wind by only considering broadband spectra of transverse Alfvén waves as drivers of the ion heating in the hybrid simulations. These waves, propagating parallel to the background magnetic field, are chosen to belong to the lower branch ($\omega < \Omega_\alpha$) of the dispersion relation of a proton-alpha-particle plasma (Sonnerup 1967) in the cold approximation:

$$k^2 - \frac{\omega}{c^2} + \frac{1}{c^2} \sum_{s=e,p,\alpha} \frac{\omega_{ps}\omega}{\omega - \Omega_s} = 0, \qquad (2)$$

where c is the speed of light, $\omega_{ps}^2 = n_s(Z_s e)^2/\epsilon_0 m_s$ and $\Omega_s = Z_s e B_0/m_s$ are the plasma and cyclotron frequencies of species s, respectively. Here, e is the magnitude of the electron charge, ϵ_0 is the vacuum permittivity, and Z_s and m_s are the atomic number and mass of ion species s (for the case of the electrons $Z_e = -1$, and $\Omega_e = -eB_0/m_e$).

Following Maneva et al. (2013), the initial configuration of the perturbed magnetic field $\delta\boldsymbol{B}(x)$ consists of $N = 31$ normal modes with wavenumbers and frequencies in the ranges $k_j d_p \in [0.017, 0.542]$ and $\omega_j/\Omega_p \in [0.015, 0.357]$, where $j = 1, \ldots, N$. Thus, the components of the perturbed magnetic field are

$$\delta B_y(x) = \sum_{j=1}^{N} B_j \cos(k_j x + \vartheta_j), \qquad (3)$$

$$\delta B_z(x) = \sum_{j=1}^{N} B_j \sin(k_j x + \vartheta_j), \qquad (4)$$

where B_j and ϑ_j are the amplitudes and initial wave-phases of the jth mode, respectively. The relationship between the initial wave-phases of the different modes determines the level of intermittency (burstiness) of the magnetic field. Each ϑ_j occurs with uniform probability in the range $[0, \theta^*]$, where θ^* is the spread in phase angles of the ϑ_j. Smaller values of θ^* result in more phase coherent waves, and hence more bursty magnetic fields, along the simulation domain. Conversely the limiting case $\theta^* = 360°$ corresponds to the random-phase approximation for the magnetic field perturbations. In this way, for a fixed power spectral density of Alfvén waves, we can obtain different levels of intermittency. Figure 1 shows three examples of magnetic fields with the same spectral density ($1/f$) but different levels of intermittency (burstiness).

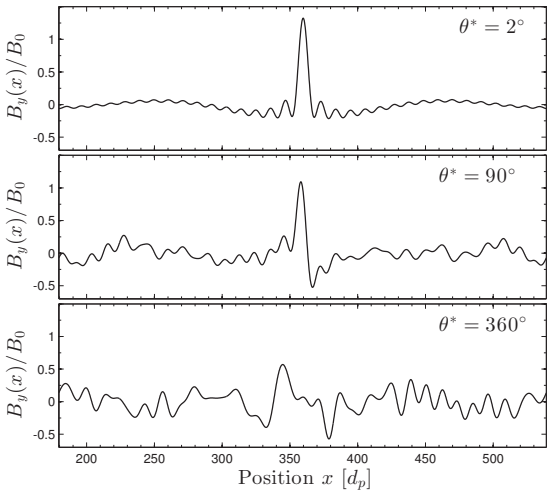

Fig. 1.— Initial condition for magnetic fields with the same power spectral density $1/f$ and three different levels of intermittency (burstiness). Subset of simulation domain shown. For simplicity, only the y component of $\delta\boldsymbol{B}(x)$ (c.f. Equation 3) is shown. Three different values of θ^* are used to specify the level of intermittency: $\theta^* = 2°, 90°$ and $360°$. The case with $\theta^* = 2°$ corresponds to the most intermittent magnetic field, whereas $\theta^* = 360°$ corresponds to the random-phase approximation for the magnetic field perturbations. All these magnetic fields contain the same total field energy.

The initial velocity distribution of protons and alpha-particles is specified to self-consistently couple the ion dynamics with the spectrum of Alfvén waves defined by Equations (3) and (4) (Sonnerup 1967; Maneva et al. 2013). This is done by intro-

ducing the following drift velocities into the initial thermalized velocity distributions of both ion species:

$$\delta u_{sy}(x) = -\sum_{j=1}^{N} \frac{\omega_j/k_j}{1-\omega_j/\Omega_s}\frac{B_j}{B_0}\cos(k_j x+\vartheta_j), \quad (5)$$

$$\delta u_{sz}(x) = -\sum_{j=1}^{N} \frac{\omega_j/k_j}{1-\omega_j/\Omega_s}\frac{B_j}{B_0}\sin(k_j x+\vartheta_j). \quad (6)$$

Here δu_s is the perturbation of the velocity distribution function of either ion species, protons or alpha-particles, $s = p, \alpha$, with respect to the Maxwellian background. In Equations (5) and (6), the wave frequencies ω_j are calculated using the dispersion relation of Equation (2) given the values of the wavenumbers k_j.

In order to compare our results with those of Maneva et al. (2013), where intermittency is not included, we chose the energy of the entire spectrum to be 6.25% of the background magnetic field energy, that is, $|\delta \boldsymbol{B}|^2/B_0^2 = 0.0625$. This corresponds to an effective amplitude of the integrated spectrum which is 25% of the magnitude of the background magnetic field. We now present the results of five hybrid simulations with different levels of intermittency.

4. SIMULATION RESULTS

We perform simulations of a $1/f^{\gamma}$ broadband spectrum of Alfvén waves relaxing in a solar wind plasma using five different values of θ^*: $2°, 90°, 180°, 270°$, and $360°$. We first describe the mechanisms responsible for the ion heating in our simulations. Then we examine the effect of these mechanisms on the local ion temperature, explain the difficulties arising if we wish to define average ion temperatures in our simulations, and discuss the implications for *in situ* observations of the intermittent solar wind. Next we study the dependence of the parallel and perpendicular ion temperature, and of temperature anisotropy, on intermittency. We also study the time evolution of the energy of protons, alpha-particles and electromagnetic fields in each case, in order to infer the effectiveness of the mechanisms driving the ion heating in relation to the intermittency level of the initial magnetic field perturbations. We then compare the results with observations of the solar wind. Finally, we study how the time evolution of the fluctuations of the ion velocity and magnetic field depend on the intermittency levels.

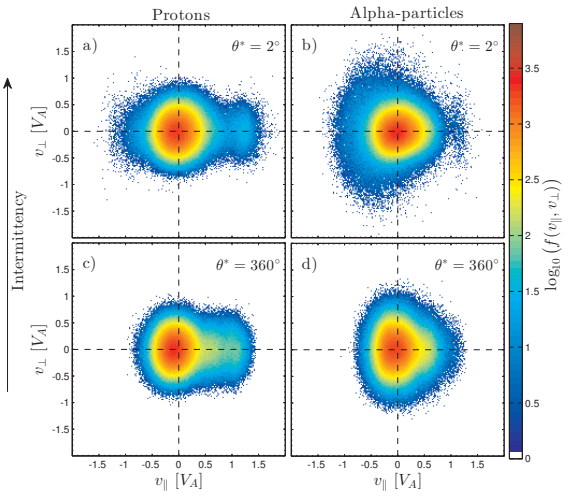

Fig. 2.— Dependence of ion velocity distribution functions on the level of intermittency. Colour shading of $\log_{10}\left(f(v_\parallel, v_\perp)\right)$ of protons and alpha-particles for two hybrid simulations at the final simulation time $t\Omega_p = 2000$. Panels a) and b) show $f(v_\parallel, v_\perp)$ of protons and alpha-particles for the hybrid simulation in the high-intermittent case $\theta^* = 2°$. Panels c) and d) show the corresponding $f(v_\parallel, v_\perp)$ for the hybrid simulation in the random phase limit $\theta^* = 360°$. The horizontal and vertical dashed lines show $v_\perp = 0$ and $v_\parallel = 0$, respectively. The ion distribution function of both ion species for the simulation with $\theta^* = 360$ shows a drift of its core anti-parallel to $\boldsymbol{B}_0$. The core of $f(v_\parallel, v_\perp)$ of the alpha-particles for the simulation with $\theta^* = 2$ shows elongation along $\boldsymbol{B}_0$. We observe the occurrence of preferential ion heating for all θ^*, i.e. all levels of intermittency. However, the features of $f(v_\parallel, v_\perp)$ in each case are different, suggesting that the mechanisms underlying the ion heating act in different ways.

4.1. Mechanisms driving ion heating in the hybrid simulations

Reconstructed velocity distribution functions $f(v_\parallel, v_\perp)$ for protons and alpha-particles of the fast solar wind show preferential heating along the ambient magnetic field (Hundhausen et al.

1967; Marsch et al. 1982a,b; Marsch 2006). This heating is seen in velocity space as an elongation of the core of $f(v_\parallel, v_\perp)$ of the protons along the perpendicular direction, together with the formation of a small beam of protons streaming approximately parallel to the ambient magnetic field with speeds comparable to the local Alfvén speed $V_A = B_0/\sqrt{\mu_0 n m_p}$. In Figure 2 we show $f(v_\parallel, v_\perp)$ for protons and alpha-particles at the final simulation time, $t\Omega_p = 2000$, for the cases where θ^* takes its two extreme values in our hybrid simulations: $\theta^* = 2°$, for highly intermittent Alfvén waves, and $\theta^* = 360°$, for random-phase Alfvén waves. In all the hybrid simulations, we observe preferential ion heating. However, the detailed features of $f(v_\parallel, v_\perp)$ differ, and have distinct time variation, for simulations that embody different levels of intermittency, suggesting that the mechanisms underlying the ion heating act in different ways (Valentini and Veltri 2009; Matteini et al. 2010).

By looking at the time evolution of both the parallel velocity $v_\parallel(x, \phi)$ as function of the ion gyro-angle $\phi = \arctan(v_\parallel/v_\perp)$, and the ion distribution function in the $xv_\parallel$-plane $f(x, v_\parallel)$, it is possible to identify the mechanisms underlying preferential ion heating in our simulations. Figure 3 shows $v_\parallel(x, \phi)$ for alpha-particles in the highly intermittent hybrid simulation with $\theta^* = 2$ at two times: the initial condition $t\Omega_p = 0$, in panel a); and at $t\Omega_p = 25$, in panel b), when heating starts to occur for this simulation. In this figure, dark red and blue colours indicate significant bunching of ions in gyro-angle space; that is, populations of alpha-particles that become phase coherent due to wave-particle interactions. Panel c) shows the corresponding $f(x, v_\parallel)$ for the alpha-particles of panel b). We also plot the normalized magnetic pressure $P_B(x) \sim \delta B^2(x)$ to show that the source of accelerated alpha-particles at $x \approx 340 d_p$ and $x \approx 390 d_p$ in panel c) is a region of high magnetic pressure ($x \approx 380 d_p - 390 d_p$). These alpha-particles are accelerated to velocities comparable to the Alfvén speed ($|v_\parallel| \sim V_A$), and can be identified as the populations of gyrobunched alpha-particles of panel b). This generic wave-particle interaction, previously identified as gyrobunching (Cook et al. 2011), is one of the mechanisms driving ion heating in our simulations. Gyrobunching is also observed for protons, and is present in all our simulations where very intense regions of magnetic pressure occur.

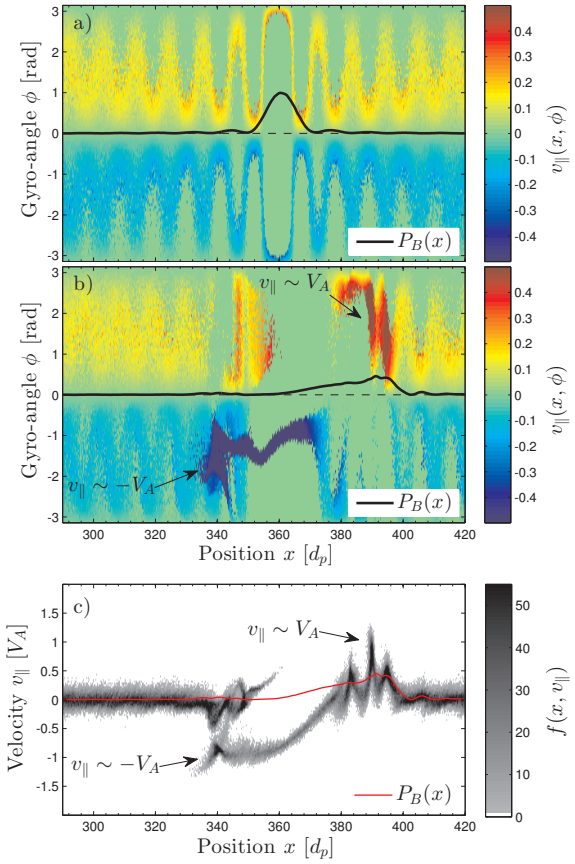

Fig. 3.— Alpha-particle acceleration due to gyrobunching in the hybrid simulation where $\theta^* = 2°$. Panels a) and b) show the colour shading of the parallel velocity $v_\parallel(x, \phi)$, where $\phi = \arctan(v_\parallel/v_\perp)$ is the ion gyro-angle, for the initial condition $t\Omega_p = 0$ and $t\Omega_p = 25.07$, respectively. Dark red and blue colours indicate significant bunching of ions in gyro-angle space. Panel c) shows $f(x, v_\parallel)$ for panel b). Alpha-particles accelerated to velocities $|v_\parallel| \sim V_A$ around regions of high magnetic pressure ($x \approx 380 d_p$), can be identified as the alpha-particle populations bunched in gyro-angle space in panel b). Gyrobunching for protons and alpha-particles is seen in all the simulations.

In Figure 4 we show $f(x, v_\parallel)$ for the protons (left panels) and alpha-particles (right panels) in three hybrid simulations with different levels of intermittency at the simulation time $t\Omega_p = 25.07$. In this figure we also show the normalized magnetic pressure $P_B(x)$ in dark blue and the normalized total particle density $n(x)/n_e$ in

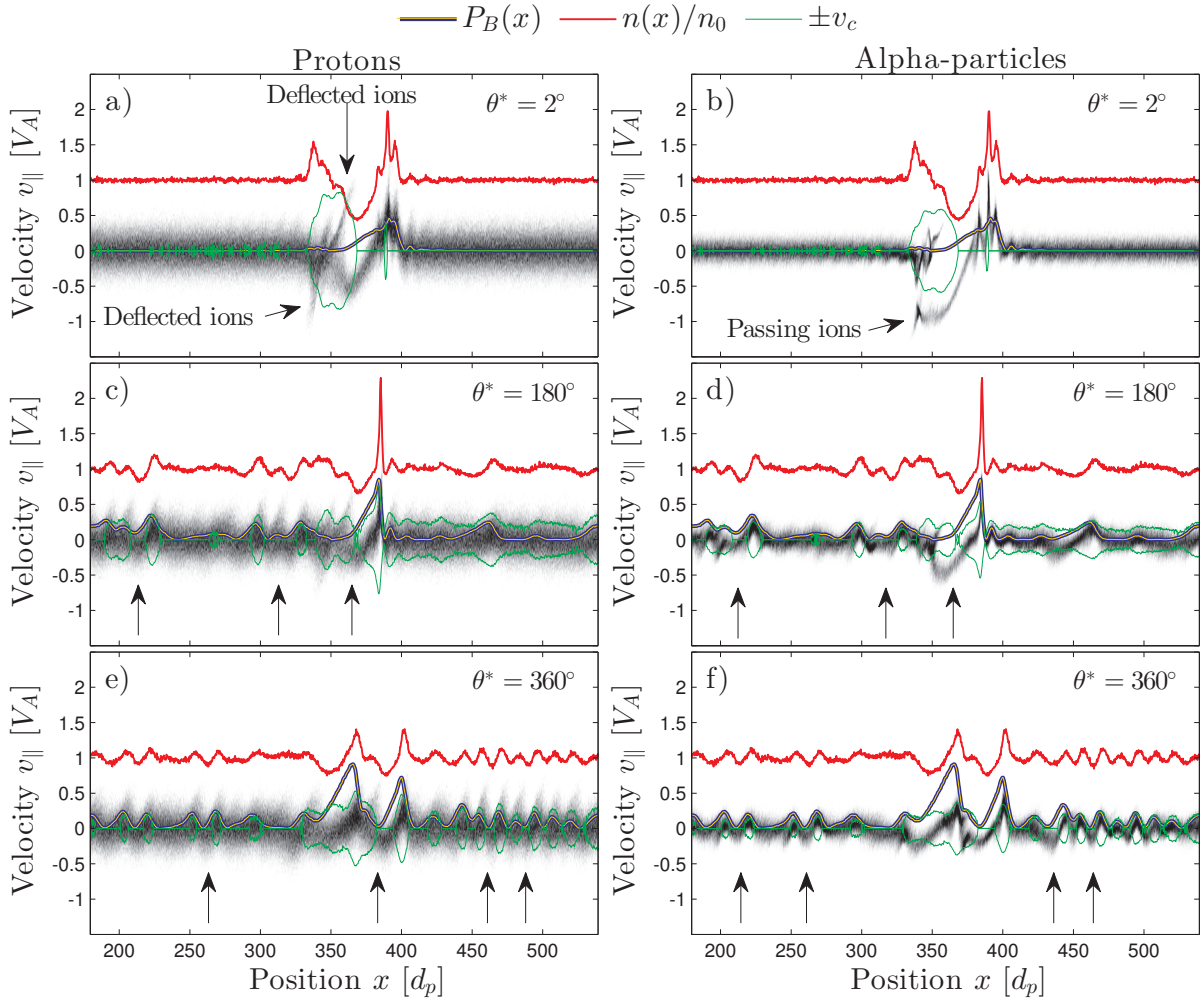

Fig. 4.— Grey scale plot of the ion distribution function $f(v_\parallel, x)$ of protons (left column) and alpha-particles (right column) at $t\Omega_p = 25.07$. Darker areas in each panel represent larger $f(v_\parallel, x)$. Along with $f(v_\parallel, x)$ we show the normalized magnetic pressure $P_B(x) \sim B^2(x)$ in dark blue, the normalized particle density $n(x)/n_e$ in red, and the critical ion velocity $\pm v_c$ in green. The magnetic pressure $P_B(x)$ is normalized to one. These quantities allow us to identify gyrobunching and ion trapping by the electric field, notably in the regions marked by arrows in panels c) to f), as the mechanisms which drive the ion heating in all the simulations. Gyrobunching and ion trapping work together, accelerating protons and alpha-particles in all the simulations shown, independent of the intermittency level of the magnetic fields. However, the specific dynamics of these mechanisms do depend on the levels of intermittency.

red. Gyrobunching generates perturbations in the ion number density $n(x)/n_e$ in our simulations, which in turn generate intense parallel electric fields $E_x(x)$ through the last term of Eq. (1). In this situation, the dynamics of ions streaming along $\boldsymbol{B}_0$ is perturbed in different ways by $E_x(x)$, depending on their kinetic energy: passing through regions of intense electric field if they have sufficiently large kinetic energy, or being trapped or deflected by $E_x(x)$ if their kinetic energy is small compared to the local electric potential energy. We can identify the regions where ion reflection or ion trapping occur by calculating the electric potential $\varphi(x) = \int_{x_0}^{x} E_x(x')dx'$, where x_0 is assumed to be far away from any perturbation. From $\varphi(x)$ we can define a threshold value

$v_{cj}(x) = \sqrt{2eZ_j\varphi(x)/m_j}$ for the ion parallel velocity $v_{\parallel j}$ of species j, such that an ion initially streaming along $\boldsymbol{B}_0$ with $\mid v_{\parallel j} \mid < v_c$ will be deflected or trapped by $E_x(x)$. However, ions with $\mid v_{\parallel j} \mid > v_c$ will continue streaming along $\boldsymbol{B}_0$ without being significantly perturbed by the parallel electric field. In Figure 4 we show v_c, for ions initially streaming parallel to $\boldsymbol{B}_0$, and $-v_c$, for ions initially streaming anti-parallel to $\boldsymbol{B}_0$. In panels a) and b) we see that protons are deflected by the intense electric field around $x \approx 350d_p$, whereas alpha-particles previously accelerated through gyrobunching (c.f. Figure 3) have acquired enough kinetic energy to pass through the region of intense $E_x(x)$ around $x \approx 350d_p$. When intense parallel electric fields occur in two contiguous regions, an ion trapping region forms. In panels c) to f) of Figure 4, we indicate with arrows some regions where ion trapping occurs. For all the values of θ^* considered, ion trapping by the electric field is observed; this mechanism seems to be more effective for Alfvén waves with initial random phases, e.g. panel e) of Figure 4.

Together, the quantities $v_\parallel(x,\phi)$, $f(x,v_\parallel)$, $P_B(x)$, $n(x)$ and $v_c(x)$, enable us to identify gyrobunching and ion trapping by the electric field as the mechanisms driving the preferential ion heating in our hybrid simulations of the solar wind. How these mechanisms operate to heat the plasma can be summarized as follows. At early times, protons and alpha-particles are accelerated along the background magnetic field due to gyrobunching in the regions of high magnetic pressure along the simulation domain, as shown in Figure 3. This acceleration produces significant fluctuations in the plasma number density $n(x)$, which at the same time generates parallel electric fields $E_x(x)$ that can trap ions. This process repeats during the simulation, eventually providing the ions with enough kinetic energy so they can escape the trapping regions and form the ion beams observed in Figure 2.

4.2. Ion energisation

Gyrobunching and ion trapping work together to accelerate protons and alpha-particles along the background magnetic field in the hybrid simulations, regardless of the level of intermittency of the broadband spectra of Alfvén waves driving the ion heating. Different levels of intermittency of the magnetic field fluctuations produce spatially inhomogeneous heating along $\boldsymbol{B}_0$, which is different in each case. Figure 5 shows the normalised local proton and alpha-particle parallel temperatures $T_{s\parallel}(x,t) = m_s\langle\delta v_{s\parallel}^2\rangle/m_pV_A^2$ at $t\Omega_p = 25.07$, panels a) to c), and at the final simulation time $t\Omega_p = 2000$, panels d) to f). In order to calculate the local $T_{s\parallel}(x,t)$, we divide the entire simulation domain into M bins, and calculate the local temperature of species s at each bin as the second statistical moment of the fluctuations of the parallel ion velocity $\delta v_{s\parallel} = v_{s\parallel}(x) - \langle v_{s\parallel}(x)\rangle$, $\langle\delta v_{s\parallel}^2\rangle$, where $\langle\rangle$ is an ensemble average only over ions within each bin. For all our calculations of $T_{s\parallel}(x,t)$ we use $M = 4096$. As the burstiness of the magnetic field perturbations increases as we vary θ^* from 360° to 2°, we can see from Figure 5 that the heating of both ion species becomes more intense and localised. In panel a) of Figure 5, corresponding to the most intermittent case in our simulations, intense localised ion heating can also be seen in the region between $x \approx 330d_p$ and $x \approx 400d_p$, while in the rest of the simulation domain there are only a few other regions where ion heating occurs. In contrast, in panel c) of the same figure, corresponding to the non-intermittent case or random phase approximation for the magnetic perturbations, less intense and more spatially homogeneous heating occurs. For the case of intense localised heating, it is not possible to meaningfully define simulation average heating rates and total temperatures at early times, because the variations of the calculated total temperatures are of the same order of magnitude as their mean values. In Karimabadi et al. (2013) are found similar results of intense localised heating of electrons and ions due to coherent structures in the form of current sheets in their 2D and 3D kinetic simulations of collisionless dissipation of energy in decaying turbulence in high-temperature plasmas.

By the end of the hybrid simulations, the ion temperature becomes spatially homogeneous, and it is then possible to meaningfully define total temperatures. In Table 1, we present a summary of the final parallel and perpendicular ion temperatures of protons and alpha-particles for all the hybrid simulations with different values of the power spectral exponent γ and levels of intermittency. In Figure 6 we plot these results for the simulation with $\gamma = 1$. Panel a) shows the parallel ($T_{p\parallel}$) and

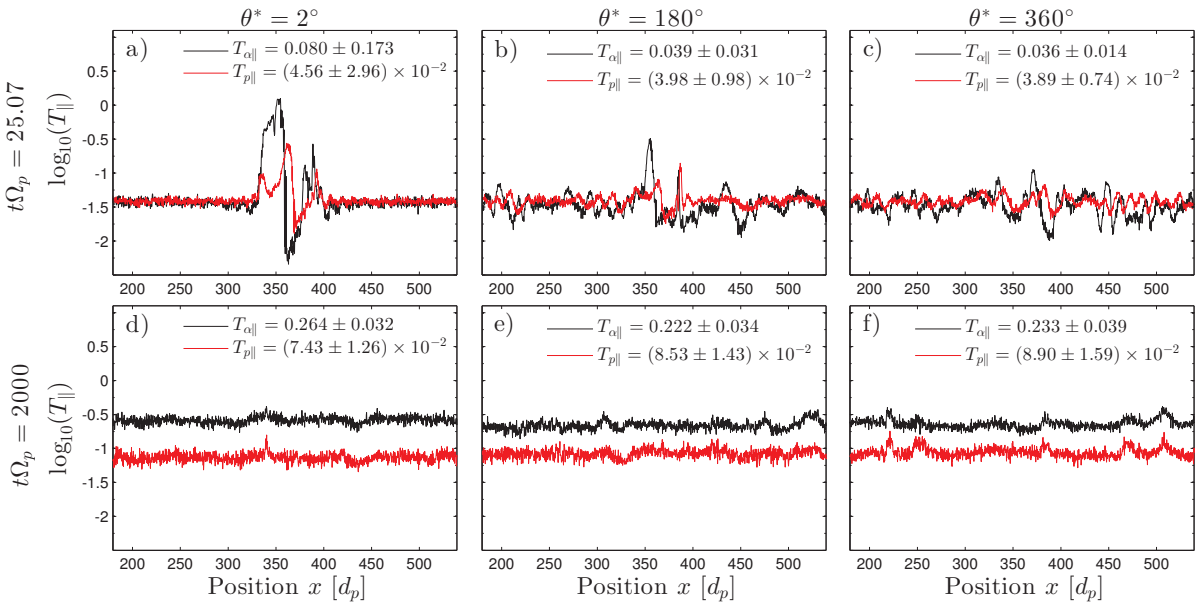

Fig. 5.— Normalised local parallel ion temperature $T_\|$ of protons and alpha-particles, plotted as a function of position at early and late times, for three different levels of intermittency. Panels a) to c) show the ion parallel temperatures at the early time $t\Omega_p = 25.07$ from the hybrid simulations with $\theta^* = 2°, 180°$ and $360°$. Intense localised heating occurs for the simulations with high levels of intermittency. Panels d) to f) show the corresponding ion parallel temperatures at final simulation time $t\Omega_p = 2000$; by this time, the heating has become homogeneous, so that average ion temperatures can be defined. The averaged proton and alpha-particle temperatures are calculated for each simulation along with their standard deviations. Large deviations from the mean value of $T_\|$ are visible at early times in all the hybrid simulations. By the end of each simulation, the ion temperatures have become more homogeneous in space.

perpendicular ($T_{p\perp}$) proton temperatures at the final simulation time ($t\Omega_p = 2000$) as functions of θ^*. We see that $T_{p\|}$ decreases with increasing intermittency level. In contrast, $T_{p\perp}$ does not vary significantly when θ^* is changed. Panel b) shows the corresponding case for alpha-particles. We see that $T_{\alpha\|}$ increases with increasing intermittency levels, whereas $T_{\alpha\perp}$ decreases. These trends are the same for different values of γ. These variations in the temperatures arise from different levels of intermittency, and this changes the values of the temperature anisotropy $T_\perp/T_\|$ for each ion species. This anisotropy is a measurable quantity in the solar wind, which can be used to compare the effects of intermittency on the preferential ion heating. In panels c) and d) of Figure 6, we show the corresponding values of $T_\perp/T_\|$ for protons and alpha-particles. In these hybrid simulations, the temperature anisotropy for protons $T_{p\perp}/T_{p\|} < 1$ always, increasing in value with increasing levels of intermittency. This is shown in Figure 6(c). The behaviour of the alpha-particles is different; for the hybrid simulations using $\theta^* = 2°$ we obtained $T_{\alpha\perp}/T_{\alpha\|} \approx 1$, independent of the value of the spectral exponent γ (inset of Figure 6(b)). For larger values of θ^* the temperature anisotropy takes values larger than one for all the values of the spectral exponent γ, that is, $T_{\alpha\perp}/T_{\alpha\|} > 1$. This is shown in Figure 6(d). Observations of the fast solar wind at about 1 AU by the Helios Solar Probes (c.f. Figure 6 of Marsch et al. (1982a)) and by Wind spacecraft (c.f. Figure 2 of Maruca et al. (2012)) show typical values of $T_{\alpha\perp}/T_{\alpha\|} \approx 1$; this is only observed in our hybrid simulations for the cases where highly intermittent magnetic field perturbations drive the ion heating. This strongly suggests that the observed values of $T_{\alpha\perp}/T_{\alpha\|}$ in the fast solar wind at 1 AU reflect a significant

degree of intermittency in the waves driving the ion heating.

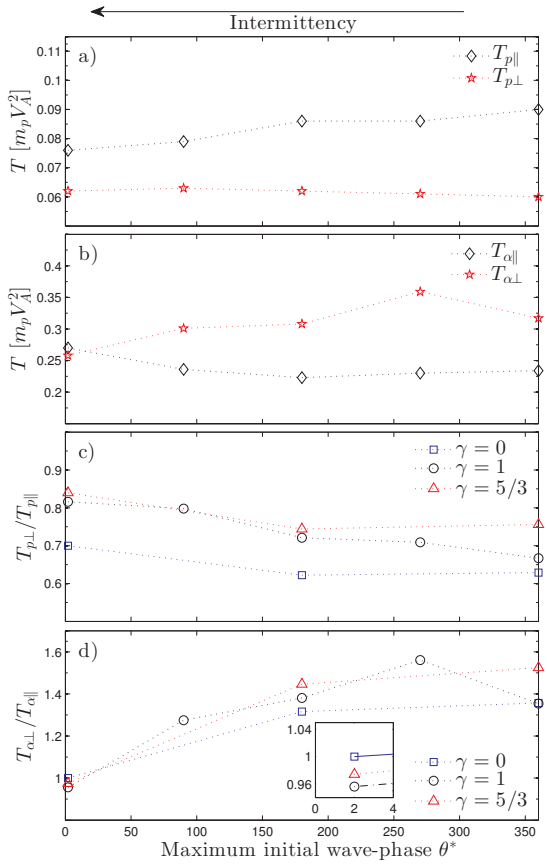

Fig. 6.— Final proton and alpha-particle temperature for different values of θ^* and γ. Panel a): final parallel (black) and perpendicular (red) proton temperature for hybrid simulations with $\gamma = 1$. Panel b): same as panel a) for alpha-particles. Panel c): proton temperature anisotropy. For protons, $T_{p\perp}/T_{p\parallel} < 1$ is always observed in our simulations, and this agrees with observations of the solar wind. Panel d): alpha-particle temperature anisotropy. For alpha-particles, the trend seen in solar wind observations is $T_{\alpha\perp}/T_{\alpha\parallel} \approx 1$; this is only observed for the hybrid simulation with $\theta^* = 2°$, independent of the value of the spectral exponent γ. The inset in this panel shows this.

In Figure 7 we plot the time evolution of the change in energy density of protons, alpha-particles and the magnetic field, for three simulations with $\gamma = 1$. This gives an indication of how strong the wave-particle interactions are in each case. The change in energy density for each ion species and the magnetic field is defined as:

$$\Delta\mathcal{E}_B = \left\langle \frac{B^2(x,t)}{2\mu_0} \right\rangle_x - \left\langle \frac{B^2(x,0)}{2\mu_0} \right\rangle_x , \quad (7)$$

$$\Delta\mathcal{E}_{K_s} = \frac{1}{L}\left[\left\langle \tfrac{1}{2} m_s v_s^2(t) \right\rangle_f - \left\langle \tfrac{1}{2} m_s v_s^2(0) \right\rangle_f \right]. \quad (8)$$

Here μ_0 is the vacuum permeability, L is the simulation domain length, and $\langle\rangle_x$ and $\langle\rangle_f$ refer to averages along the simulation domain and over the ion distribution functions, respectively. All the simulations show the same qualitative trend: at early times, the alpha-particles transfer some energy to the protons through wave-particle interactions. Then a re-energization of the alpha-particles occurs, while the protons are still being energized, although at a slower rate than at early times. By the end of the simulation that has initially random wave-phases ($\theta^* = 360°$), $\Delta\mathcal{E}_{K_p}$ saturates, that is, the protons are not energized further. However, the alpha-particles continue to gain energy. In the other hybrid simulations, which have non-zero initial intermittency, the saturation of $\Delta\mathcal{E}_{K_p}$ is not observed. The energy density of the electric field, which is of the order of magnitude of 10^{-21} J/m^3, decreases over time in all the hybrid simulations. Shown in Figure 7, all the simulations give rise to a similar final energy density of alpha-particles. The case where the initial wave-phases are random ($\theta^* = 360°$) shows the biggest decrease in magnetic field energy, together with the largest proton energy density at the end of the simulation. Conversely, the simulation with highly intermittent Alfvén waves ($\theta^* = 2°$) shows the smallest decrease in magnetic field energy and the smallest proton energy density increase. This implies that, in the former case, the alpha-particles are energised by extracting energy mostly from the magnetic field; whereas, in the latter case, the alpha-particles extract energy from the magnetic field and protons. This is observed consistently across simulations with different values of spectral exponent γ.

Summarizing, we find that different levels of intermittency lead to different temporal and spatial dynamics of the two mechanisms driving preferential ion heating in our simulations: specifically, gyrobunching and ion trapping by the elec-

Table 1: Final parallel and perpendicular temperatures of protons and alpha-particles for hybrid simulations in which ion heating is driven by broadband Alfvén wave populations that have different intermittency levels θ^* and spectral exponent γ.

θ^*	Spectral exponent γ $(1/f^\gamma)$	$T_{p\parallel}$ $[m_pV_A^2]$	$T_{p\perp}$ $[m_pV_A^2]$	$T_{\alpha\parallel}$ $[m_pV_A^2]$	$T_{\alpha\perp}$ $[m_pV_A^2]$	$T_{p\perp}/T_{p\parallel}$	$T_{\alpha\perp}/T_{\alpha\parallel}$
2	0	0.090	0.063	0.325	0.325	0.700	1.000
2	1	0.076	0.062	0.270	0.258	0.816	0.956
2	5/3	0.075	0.063	0.267	0.260	0.840	0.974
90	1	0.079	0.063	0.236	0.301	0.798	1.275
180	0	0.098	0.061	0.282	0.371	0.622	1.316
180	1	0.086	0.062	0.223	0.308	0.721	1.381
180	5/3	0.082	0.061	0.213	0.308	0.744	1.446
270	1	0.086	0.061	0.230	0.359	0.709	1.561
360	0	0.097	0.061	0.305	0.414	0.629	1.357
360	1	0.090	0.060	0.234	0.317	0.667	1.354
360	5/3	0.082	0.062	0.198	0.302	0.756	1.525

tric field. Also, the ion temperature anisotropy of protons and alpha-particles shows a strong dependence on intermittency levels. We find that intermittency does not allow a meaningful determination of average temperatures and heating rates at early times in our simulations. The net effect of random-phase Alfvén waves in our simulations is to provide a more efficient channel for energy transfer between ions and electromagnetic fields through wave-particle interactions. There are two possible factors for this: first, the wave-particle interactions that energise ions unfold faster for random-phase Alfvén waves than for highly intermittent Alfvén waves; and second, for the same total field energy, the random-phase Alfvén waves fill the simulation domain from early times, whereas the highly intermittent Alfvén wave field generates isolated regions of heating.

4.3. Correlation between ion velocity and magnetic field fluctuations

Finally, we explore the role of intermittency in the time evolution of the magnetic perturbations in the hybrid simulations. *In situ* observations of the solar wind show that the waves permeating the solar wind are mostly of Alfvénic nature (Belcher and Leverett Jr. 1971; Belcher and Solodyna 1975; Bruno et al. 1985; Bruno and Carbone 2013). That is, the ion velocity $\boldsymbol{U}_i$ and magnetic field fluctuations $\delta\boldsymbol{B}$ are correlated, and satisfy Walen's relation $\boldsymbol{U}_i = \pm C_A \delta\boldsymbol{B}$, where $C_A \approx (\mu_0 n m_p)^{-1/2}$. Here the minus (plus) sign refers to pure Alfvénic waves propagating parallel (anti-parallel) to the background magnetic field. Initially, the fluctuations of the magnetic field and ion velocity in the hybrid simulations are purely Alfénic. Then, as the plasma evolves, there can be parametric decay of the initial Alfvén waves (Araneda et al. 2008; Matteini et al. 2010, 2011), giving way to the excitation of non-Alfvénic waves that interact with the ions in different ways. We study this by calculating the time evolution of the spatial correlation of δB_y and U_{iy}, defined by

$$C(\delta B_y, U_{iy})(t) = C_0 \int_L \delta B_y(x',t) U_{iy}(x',t) dx' \ . \tag{9}$$

Here, the integral is over the entire simulation domain L, and C_0 is a constant that normalizes the correlation values between -1 and 1.

Figure 8 shows $C(\delta B_y, U_{iy})$ for the hybrid simulations that generated Figure 7. For all cases $C(\delta B_y, U_{iy}) \approx -1$ at $t\Omega_p = 0$, consistent with the initial condition of pure Alfvén waves propagating parallel to $\boldsymbol{B}_0$. For the simulation with initial random wave-phases (black), non-Alfvénic waves are excited as the system evolves in time: the magnetic and ion bulk velocity perturbations become uncorrelated, $C(\delta B_y, U_{iy}) \to 0$. Conversely, in the simulation with initially highly intermittent

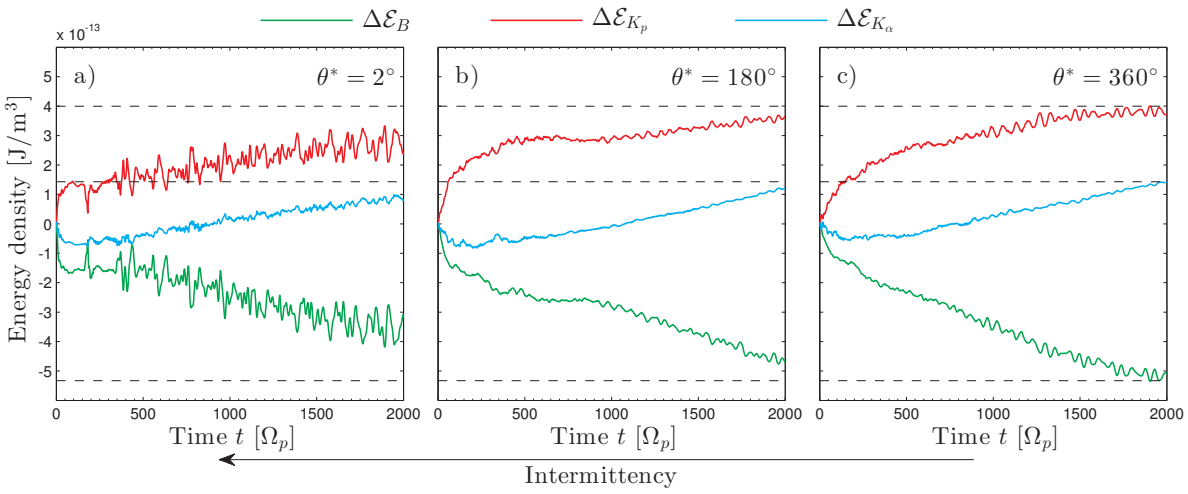

Fig. 7.— Time evolution of change in ion energy density and magnetic field energy density for hybrid simulations, all with an initial $1/f$ broadband spectrum of Alfvén waves, but with different levels of intermittency. From top to bottom: the change in proton energy density $\Delta\mathcal{E}_{K_p}$ (red), the change in alpha-particle energy density $\Delta\mathcal{E}_{K_\alpha}$ (cyan), and the change in magnetic field energy density $\Delta\mathcal{E}_B$ (green). The horizontal dashed lines are plotted only to assist comparison of $\mathcal{E}_{K_p}$, $\Delta\mathcal{E}_{K_\alpha}$ and $\Delta\mathcal{E}_B$ across the different hybrid simulations. All the simulations show the same qualitative trends. At early times, the alpha-particles transfer some energy to the protons through wave-particle interactions. Thereafter there is re-energization of the alpha-particles, while the protons continue to be energized, but at a slower rate. $\Delta\mathcal{E}_{K_p}$ saturates by the end of the simulation time. There is a regular decline in magnetic field energy density.

Alfvén waves (blue), these remain mostly Alfvénic during the simulation; that is, $C(\delta B_y, U_{iy})$ does not departs significantly from -1.

Summarizing, we find that the dynamics of the ion bulk velocity and magnetic field fluctuations depend on intermittency levels of the electromagnetic fields. Walen's relation holds for long times only when intermittency is included.

5. CONCLUSIONS

We have performed the first study of preferential ion heating driven by $1/f^\gamma$ broadband spectra of Alfvén waves that have different levels of intermittency for a given value of the spectral exponent γ. Intermittency is incorporated in our model through non-random phase relationships between the modes which together comprise an initial $1/f^\gamma$ spectrum of Alfvén waves. Our hybrid simulations resolve the full kinetic dynamics of ions, allowing us to study in detail the effects of intermittency on the mechanisms that might be responsible for the observed preferential ion heating in the fast solar wind.

We find that:

- Gyrobunching and ion trapping by the electric field are the two mechanisms underlying preferential ion heating in our simulations (Figures 3 and 4).
- Different levels of intermittencyfor a given broadband spectrum of Alfvén waves lead to different temporal and spatial dynamics of the mechanisms underlying preferential ion heating (Figure 2).
- The proton and alpha-particle temperature anisotropy $T_\perp/T_\parallel$ shows strong dependence on the level of intermittency of the electromagnetic fields. We find $T_{p\perp}/T_{p\parallel} < 1$ in all our simulations, decreasing in value as the intermittency level increases; and $T_{\alpha\perp}/T_{\alpha\parallel} > 1$ for all the values of θ^* except for the most intermittent case $\theta^* = 2°$. This result, $T_{\alpha\perp}/T_{\alpha\parallel} \approx 1$, is consistent with what is typically seen in observations (Marsch et al. 1982a,b; Maruca et al. 2012; Maruca B. A. 2012).

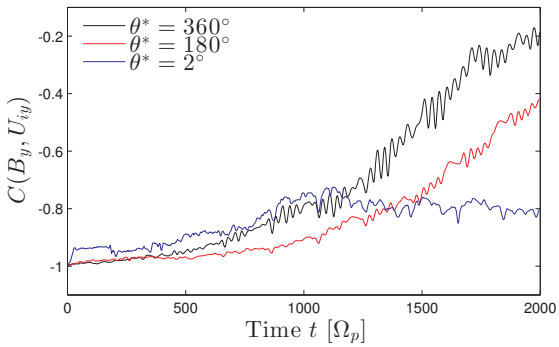

Fig. 8.— Time evolution of the spatial correlation between the ion velocity and magnetic field fluctuations in the hybrid simulations of the solar wind. Initially, $C(\delta B_y, U_{iy}) \approx -1$, consistent with the initial condition of pure Alfvén waves propagating parallel to $\boldsymbol{B}_0$. For the case where the initial wave-phases are random (black): $\theta^* = 360°$ the broadband spectrum of Alfvén waves decay into non-Alfvénic waves, that is, $C(\delta B_y, U_{iy}) \to 0$. In the case with highly intermittent Alfvén waves (blue): $\theta^* = 2°$ the plasma waves remain mostly Alfvénic throughout the simulation.

- The net effect of random-phase, hence non-intermittent, Alfvén waves in our simulations is to provide a more efficient channel for energy transfer between ions and electromagnetic fields through wave-particle interactions. This may result from the fast time scales at which the wave-particle interactions that energise ions unfold; and from how the random-phase Alfvén waves fill the simulation domain at early times. On the other hand, highly intermittent Alfvén waves generate isolated regions of heating, and this seems to favour energy transfer from protons to alpha-particles (Figure 7).

- The dynamics of the velocity and magnetic field fluctuations depend on the initial level of intermittency of the broadband spectrum of Alfvén waves driving the heating. Walen's relation $\boldsymbol{U}_i = \pm C_A \delta \boldsymbol{B}$ holds for long times only when intermittency is included (Figure 8).

- Intermittent Alfvén waves produce strong localised heating (Figure 5), and in consequence we cannot meaningfully define average heating rates and total temperatures at early times in our simulations. This suggests that in the intermittent solar wind similar localised heating might occur, making difficult to obtain good estimates of mean ion temperatures and ion heating rates, which later are used in theoretical and numerical modelling of the solar wind.

- Our results do not in general show any trend with different spectral exponents γ, consistent with Maneva et al. (2013). The only clear trend, as expected, relates to the energy transfer between the magnetic field and the alpha-particles, which is found to be larger (smaller) for $\gamma = 0$ ($\gamma = 5/3$). This follows from the fact that for $\gamma = 0$ ($\gamma = 5/3$) there is more (less) energy available at modes close to ion cyclotron resonance, that is, $\omega \sim \Omega_\alpha$.

There is good agreement between our results and Maneva et al. (2013) for the case where the broadband spectrum of Alfvén waves is random-phase. They found that if solar wind expansion is included in the simulations, the value of $T_{\alpha\perp}/T_{\alpha\parallel}$ decreases. This suggests that simulations that include both intermittency and solar wind expansion, might lead to values of $T_{\alpha\perp}/T_{\alpha\parallel}$ closer to typical observation values of $T_{\alpha\perp}/T_{\alpha\parallel}$.

The present study represents the first attempt to investigate the role of intermittency in the heating of the solar wind. We do not attempt to capture specific intermittency properties of the observed solar wind. Future work might include the use of more realistic models of intermittency to generate the broadband spectra of Alfvén waves to drive the heating (Subedi et al. 2014).

Acknowledgements

The authors thank the MPIPKS, Dresden for support. L.C. acknowledges L. Matteini for discussion, the Mexican Council of Science and Technology (CONACyT), and the Royal Astronomical Society (RAS) for support. SCC acknowledges the STFC.

REFERENCES

Alexandrova, O., Chen, C. H. K., Sorriso-Valvo, L., Horbury, T. S. and Bale, S. D. 2013, Space Sci. Rev. **178**, 101.

Araneda, J. A., Marsch, E. and F.-Vias, A. 2008, Phys. Rev. Lett. **100**, 125003.

Araneda, J. and Maneva, Y. and Marsch, E. 2009, Phys. Rev. Lett. **102**, 175001.

Belcher, J. W. and Leverett, D. Jr. 1971, J. Geophys. Res **76**, 3534.

Belcher, J. W. and Solodyna, C. V. 1975, J. Geophys. Res **80**, 181.

Bruno, R., Bavassano, B. and Villante, U. 1985, J. Geophys. Res **90**, 4373.

Bruno, R., Carbone, V., Chapman, S., Hnat, B., Noullez, A., and Sorriso-Valvo, L. 2007, Phys. Plasmas, **14**, 032901.

Bruno, R., Carbone, V., Vörös, Z., D'Amicis, R., Bavassano, B., Cattaneo, M. B., Mura, A., Milillo, A., Orsini, S., Veltri, P., Sorriso-Valvo, L., Zhang, T., Biernat, H., Rucker, H., Baumjohann, W., Jankovičová, D. and Kovács, P. 2009, Earth, Moon, and Planets **104**, 101.

Bruno, R. and Carbone, V. 2013 , Living Rev. Solar Phys. **10**, 2.

Carbajal, L., Dendy, R. O., Chapman, S. C. and Cook, J. W. S. 2014, Phys. Plasmas **21**, 012106.

Clark, S. E., Winske, D., Schaeffer, D. B., Everson, E. T., Bondarenko, A. S., Constantin, C. G., and Niemann, C. 2013, Phys. Plasmas **20**, 082129.

Cook, J. W. S., Dendy, R. O. and Chapman, S. C. 2011, Plasma Phys. and Control. Fusion **53**, 074019.

De Pontieu, B., Mcintosh, S. W., Carlsson, M., Hansteen, V. H., Tarbell, T. D., Schrijver, C. J., Title, A. M., Shine, R. A., Tsuneta, S., Katsukawa, Y., Ichimoto, K., Suematsu, Y., Shimizu, T. and Nagata, S. 2007, Science **318**, 1574.

Goldstein, B. E., Smith, E. J., Balogh, A., Horbury, T. S., Goldstein, M. L. and Roberts, D. A. 1995, Geophys. Res. Lett. **22**, 3393.

Gurnett, D. A., Marsch, E., Pilipp, W., Schwenn, R. and Rosenbauer, H. 1979, J. Geophys. Res. **84**, 2029.

Hnat, B., Chapman, S. C., Rowlands, G., Watkins, N. W. and Farrell, W. M. 2002, Geophys. Rev. Lett. **29**, 86.

Hnat, B., Chapman, S. C. and Rowlands, G. 2003, Phys. Rev. E **67**, 056404.

Horbury, T. S., Forman, M. A. and Oughton, S. 2005, Plasma Phys. Cont. Fusion. **47**, B703.

Hundhausen, A. J., Asbridge, J. R., Bame, S. J. and Strong, I. B. 1967, J. Geophys. Res. **72**, 1979.

Karimabadi, H., Roytershteyn, V., Wan, M., Matthaeus, W. H., Daughton, W., Wu, P., Shay, M., Loring, B., Borovsky, J., Leonardis, E., Chapman, S. C. and Nakamura, T. K. M. 2013, Phys. Plasmas **20**, 012303.

Liewer, P. C., Velli, M. and Goldstein, B. E 2001, J. Geophys. Res. **106**, 261.

Maneva, Y. G., Viñas, A. F. and Ofman, L. 2013, Journal of Geophysical Research: Space Physics **118**, 2169-9402.

Marsch, E., Muhlhauser, K.-H., Schwenn, R., Rosenbauer, H. and Neubauer, F. M. 1982a, J. Geophys. Res **87**, 35.

Marsch, E., Muhlhauser, K.-H., Schwenn, R., Rosenbauer, H., Pilipp, W. and Neubauer, F. M. 1982b, J. Geophys. Res **87**, 52.

Marsch, E. and Tu, C.-Y. 1990, J. Geophys. Res **89**, 8211.

Marsch, E. 2006, Living Rev. Solar Phys. **3**, 1.

Maruca, B. A., Kasper, J. C. and Gary, S. P. 2012, ApJ **748**, 137.

Maruca. B. A. 2012, PhD Thesis, Harvard University.

Matteini, L., Landi, S., Velli, M., Hellinger, P. 2010, J. Geophys. Res. **115**, A09106.

Matteini, L., Hellinger, P., Landi, S., Trávníček, P. M. and Velli, M. 2011, Space Sci. Rev. **172**, 373.

Matthaeus, H. and Goldstein, M. L. 1986, Phys. Rev. Lett. **57**, 495.

Nariyuki, Y., Hada, T. and Tsubouchi, K. 2010, Phys. Plasmas **17**, 072301.

Nariyuki, Y., Umeda, T., Suzuki, T. K. and Hada, T. 2014, Nonlinear Processes Geophys. **21**, 339.

Nicol, R., Chapman, S. C. and Dendy, R. O. 2009, ApJ, **703**, 2138.

Ofman, L., Gary, S. P. and Viñas, A. 2002, J. Geophys. Res **107**, 1461.

Ofman, L. 2004, J. Geophys. Res **109**, A07102.

Osman, K. T., Matthaeus, W. H., Greco, A. and Servidio, S. 2011, ApJ Lett. **727**, L11.

Osman, K. T., Matthaeus, W. H., Wan, M. and Rappazzo, A. F. 2012, Phys. Rev. Lett. **108**, 261102.

Osman, K. T., Kiyani, K. H., Chapman, S. C. and Hnat, B. 2014, ApJ Lett. **783**, L27.

Perrone, D., Valentini, F., Servidio, S., Dalena, S. and Veltri, P. 2013, ApJ **762**, 99.

Pritchett, P. L. 2000, IEEE Transactions on Plasma Science **28**, 1976-1990.

Sonnerup, B. U. Ö. 1967, Phys. Fluids **10**, 462.

Subedi, P. and Chhiber, R. and Tessein, J. A., Wan, M. and Matthaeus, W. H. 2014, ApJ **796**, 97.

Taylor, G. I. 1938, Proc. R. Soc. Lond. A **164**, 476.

Valentini, F., Veltri, P., Califano, F. and Mangeney, A. 2008, Phys. Rev. Lett. **101**, 025006.

Valentini, F. and Veltri, P. 2009, Phys. Rev. Lett. **102**, 225001.

Veltri, P. 1999, Plasma Phys. Controlled Fusion **41**, A787.

Verdini, A., Grappin, R., Pinto, R. and Velli, M. 2012, ApJ Lett. **750**, L33 .

Winske, D. and Omidi, N. 1996, Journal of Geophysical Research: Space Physics **101**, 17287-17303.

Wu, P., Perri, S., Osman, K., Wan, M., Matthaeus, W. H., Shay, M. A., Goldstein, M. L., Karimabadi, H., and Chapman, S. C. 2013, ApJ Lett. **763**, L30.

This 2-column preprint was prepared with the AAS LaTeX macros v5.2.